THE STRUCTURE AND PROPERTIES OF THE NANOCOMPOSITE FILMS NB-AL-N

V I Ivashenko[1], A D Pogrebnyak[2], P L Skrinski[1], V N Rogoz[2], S V Plotnikov[3], N K Erdybaeva[3], E O Tleukenov[3]

[1] *Institute of Materials Science problems, Kryzhanovskaya Street. 3, 03680, Kiev-142, Ukraine*

[2] *Sumy State University, Rimsky-Korsakov Street, 2, 40000, Sumy, Ukraine*

3 D. Serikbayev East Kazakhstan State Technical University, 23/2-54 Serikbayev Street, 070003, Ust-Kamenogorsk, Kazakhstan

alexp@i.ua

Abstract

Nanocomposite films Nb-Al-N produced by magnetron sputtering were researched in this work. Two stable crystalline structural states were found in the films: NbN_{ch} and solid solution B1−$Nb_xAl_{1-x}N_yO_{1-y}$, and also an amorphous component associated with aluminum oxynitride with reactive magnetron sputtering. Sensitivity of substructural characteristics was set up to the current supplied to Al target and their relationship with the characteristic nanohardness and Knoop hardness. Recent changes in the range of 29-33.5 GPa and 46-48 GPa, respectively. Initial principle calculations of phases NbN and Nb_2AlN and also heterostructures of NbN/AlN were carried out for the interpretation of the results. The work was performed as a part of two complex state programs: "Development of nanostructured superhard coatings formation foundations with high physical-mechanical properties" (number 0112u001382) and "Physical principles of plasma technologies for complex processing of multicomponent materials and coatings" (number 0113u000137c).

1. INTRODUCTION

Films based on NbN show many interesting properties such as high hardness and electrical conductivity, thermal stability and chemical inertness. [1] NbN films are used as the cathode material for field electron emission in vacuum of microelectronic devices [2]. It was shown that the introduction of Al atoms into the lattice led to the formation of solid solution $Nb_{1-x}Al_xN$. For solid solutions $Nb_{1-x}Al_xN$, B1 (type - NaCl) structure is more preferable for x below 0.45. In the range of x = 0.45-0.71, the mixture of structures B1 and B4 was observed, while when x> 0.71, B4 structure (type - wurtzite with a hexagonal structure) was formed [6,7]. Films Nb-Al-N composed of solid solution $Nb_{1-x}Al_xN$ with B1 (rare B_K) and B4 structures or mixtures thereof [3-7]. On the other hand, hitherto, nanocomposite NbN/AlN films were not investigated. Thus, in the present study, we set out to research the Nb-Al-N film, arguing that under certain conditions can be formed nanocomposite structure of the films, which may have improved mechanical properties compared to films composed of the substitutional solid solutions $Nb_{1-x}Al_xN$.

2. EXPERIMENTAL DETAILS

Films Nb-Al-N deposited on the mirror-polished wafer Si (100) using a DC magnetron sputtering Nb (99.9%, Ø72 x 4 mm) and Al (99.999%, Ø72 x 4 mm) under argon and nitrogen with the following parameters of deposition: the substrate temperature T_S = 350°C; substrate bias voltage U_B = -50 V; The flow rate (F) F_{Ar} = 40 sccm; F_{N2} = 13 sccm; operating pressure P_C = 0.17 Pa. The current supplied to the target Al (I_{Al}) was 100, 150, 200, 250 and 300 mA, which corresponds to the discharge power density P_{Al} = 5.7, 8.6, 11.4, 13.7 and 17.1 W/cm^2, respectively. Current supplied to the target Nb (I_{Nb}) was 300 mA (P_{Nb} = 17.1 W/cm^2). The base pressure in the vacuum chamber was better than 10^{-4} Pa. The distance between the target and the substrate holder was 8 cm. The dihedral angle between the targets was ~ 45^0. Substrates were

ultrasonically cleaned before they were placed in a vacuum chamber. Furthermore, prior to deposition, the substrates were etched in a vacuum chamber in the hydrogen plasma for 5 min.

3. RESULTS AND DISCUSSION

Structural and mechanical properties were analyzed depending on I_{Al}.values. The structure of the coatings was researched by X-ray diffraction (XRD, diffractometer DRON-3M) in CuK_{α} radiation. The program of authoring profiles sharing was used with the application of complex diffraction profiles. Substructural characteristics (crystallite and microstrain size) were determined by approximation using the approximation function as - Cauchy function. The spectrum of Fourier spectroscopy (FTIR) was measured at room temperature in the range of 400−4000 cm^{-1} by spectrometer "TSM 1202" LTD «Infraspek». Knoop hardness (HK) was assessed using microhardnessmeter Microhardness Tester Micromet 2103 BUEHLER LTD under a load of 100 mN, and by nanoindentation using nanohardnessmeter G-200, equipped with a Berkovich indenter. The loads were chosen in such conditions that the indenter penetration wouldn't exceed 10-20% of the film hickness. The film thickness was determined by optical profilometer "Micron-gamma". The thickness of the Nb-Al-N coatings (d) depends weakly on I_{Al}. D values were in the range of 0.7-0.9 μm.

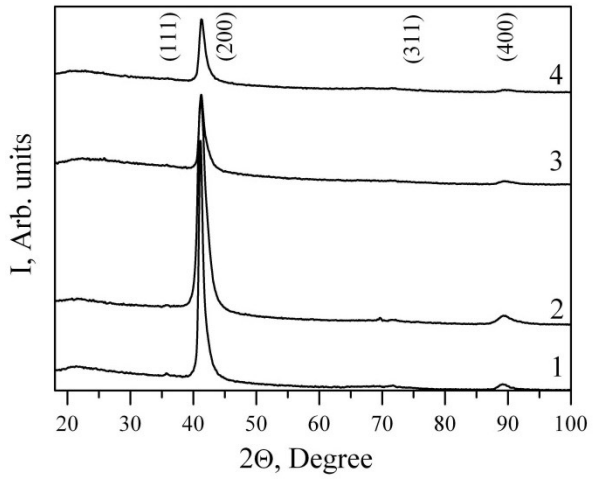

(a)

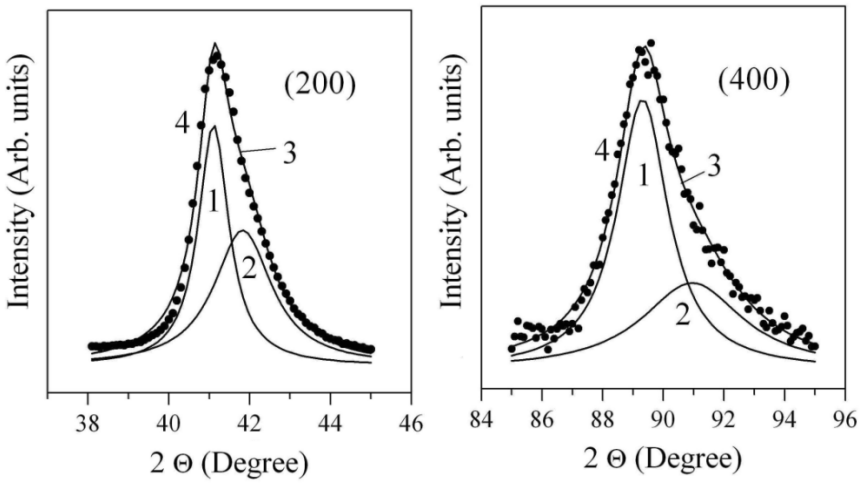

(b)

Fi 1. XRD spectra of Nb-Al-N coatings deposited at different I_{Al}: 1 − 100 mA, 2 − 150 mA, 3 − 250 mA, 4 – 300 mA (a) portion and on the division of the diffraction profile of coating components Nb-Al -N, deposited at I_{Al} = 150 mA (b): 1 − NbN, 2 − $Nb_{0,67}Al_{0,33}N$, 3 - total approximating curve, 4 - starting point of the data array.

Figure 1 (a) shows the X-ray diffraction spectra of the Nb-Al-N films at various I_{Al}. Marked peaks correspond to the structure of the planes B1−NbN_x [8]. Halo component of the amorphous phase was manifested at the same time in the range of diffraction angles 2Θ = 18−30°, based on previous studies halo component can be identified as the amorphous phase of aluminum nitride. It is seen that the reflection (200) is the main comparing with others. Crystallites were formed for all I_{Al} with a relatively small constant potential of bias on the substrate -50 V with preferentially oriented growth with [100] axis perpendicular to the plane surface. The X-ray (200) and (400) reflections are asymmetrical to larger angles . Separating these reflexes showed the presence of two components with similar lattice type, but with two typical periods. Figure 1 (b) shows the results of the deconvolution of (200) and (400) peaks in the Gaussian for the film deposited at 150 mA (curve 1 in Figure 1 (a)). Curves 1 in Figure 1 (b) correspond to the cubic niobium nitride with lattice constant a = 0.439-0.438 nm. Gaussian curve 2 can be attributed to a cubic NbN with low aluminum content and the type of substitution = 0.428-0.429 nm, which is characteristic of the system Ti-Al-N with ratio of aluminum and niobium atoms in the lattice as 1/2 (approximate composition is $Nb_{0,67}Al_{0,33}N$). The latest one was determined based on the Vegard's rule for the same type of crystal lattices by substitution of atoms with different radius [9]. Along with this, lattice parameters B1-NbNx and B1-AlN were used as the basic, respectively 0.4393 nm and 0.4120 nm [5]. With increasing I_{Al} Gaussian peak position does not change, and the intensity of the peaks associated with the solid solution increases. For higher currents, the phase relationship $NbN_x/Nb_{0.67}Al_{0.33}N$ is in proportion close to 5.3.

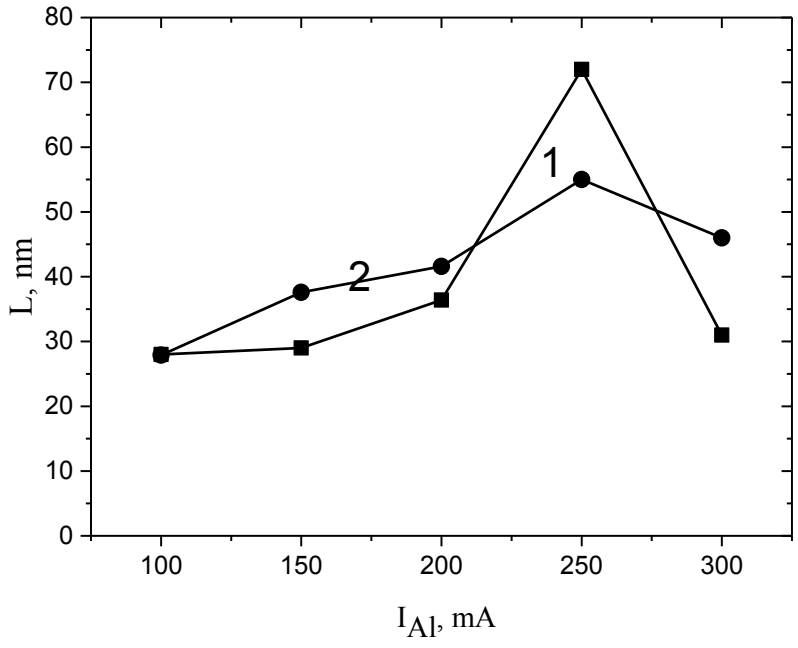

(a)

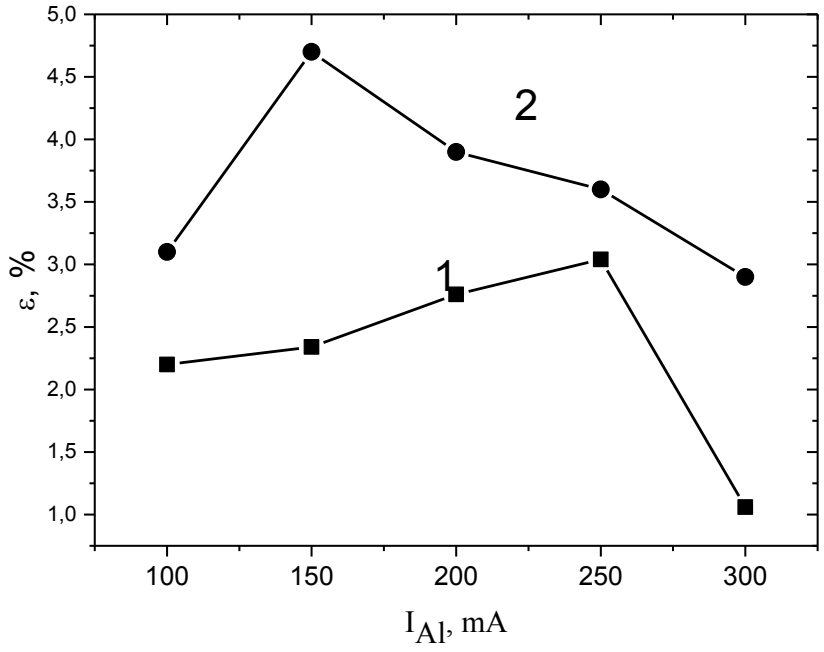

(b)

Fig. 2. The dependence of the substructural characteristics (average crystallite size, L (a) and microdeformation, ε (b)) on I_{Al} for 1 − NbN and 2 − $Nb_{0.67}Al_{0.33}N$ (or (Nb_2AlN) crystalline components.

The method of approximation was used to determine the substructural characteristics of two diffraction reflections orders. A pair of (200)-(400) also was used. The results of determination of substructural characteristics are shown in Figure 2. It can be seen that as the current increases in the direction of the axis I_{Al} texture [100], there is an increase in crystallite size and micro deformation state of them. Latest one apparently is determined by large dissolving of aluminum atoms in the lattice of niobium, which leads to a strong distortion of the lattice. The sharp decrease in crystallite size and microstrain values at the maximum current of I_{Al} = 300 mA may be due to the annealing process and the ordering of the defect structure with the formation of new boundaries on the type of process polygonization.

We deposited AlN films at various I_{Al}. X-ray studies showed that all AlN films were amorphous (a-AlN, is not shown in the paper). Infrared absorption spectra of AlN films indicate that the number of Al-N bonds increases with I_{Al} enhancement: (zone of absorption at 667 cm^{-1}, associated with fluctuations of Al−N [10] becomes more noticeable).

On the basis of these results, it can be assumed that two stable crystalline structural states were found in the films: B1−NbN_x and solid solution with a composition close to the B1−$Nb_{0.67}Al_{0.33}N$. The films also contain an amorphous component associated with aluminum nitride. Thus, the films have a nanocomposite structure which is nanocrystallites- B1−NbN_x и B1−$Nb_xAl_{1-x}N$ embedded in a matrix of a-AlN (nc−B1−NbN_x/nc−B1−$Nb_xAl_{1-x}N$/a−AlN).

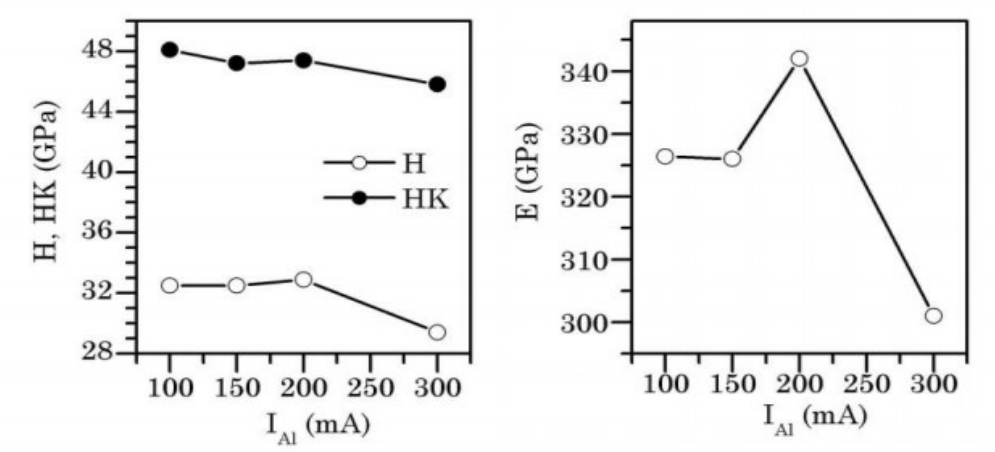

Figure 3. Nanohardness (H), the Knoop hardness (HK)(a) and modulus of elasticity (E)(b) depending on I_{Al}.

The results of nanoindentation and microindentation deposited films are shown in Figure 3. Comparison of the results in Figure 2 and 3 shows that there is a correlation between the mechanical properties and microdeformations in the Nb-Al-N films. Also nanohardness, elastic modulus and Knoop hardness (HK) are maximum for films Nb-Al-N with a grain size in the range of 30-40 nm. Increase of nanohardness from 28 GPa for films NbN [11] to 32 GPa for the Nb-Al-N film is obviously connected with the formation of a nanocomposite tipped Nb-Al-N film. We observed that the Knoop hardness higher than nanohardness ~ 50%. This may be due to the fact that the nanoindentation occurs dynamically, while the Knoop hardness is determined in a static mode. In order to verify our conclusions on the structure of Nb-Al-N films we performed initial principal calculations of B1 -NbN, solid solutions B1−$Nb_xAl_{1-x}N$, heterostructures B1−NbN(001)/B1−AlN and the ordered phase Nb_2AlN. Terms of calculation are described in detail in the work [12]. Here we note that the calculations were performed using the computational code [13]. A generalized gradient approximation was used for exchange correlational potential [14]. Simulation of molecular dynamics was performed using NVT ensemble at 1400 K with subsequent cooling to 0 K and with static relaxation [12].

96 atomic structures built by translating 8-nuclear-cell B1 as (2×2×3) were considered [12]. The compositions of solid solutions and heterostructures were selected equally. Nb_2AlN cell (space group $P6_3/mmc$, No. 194) consists of eight atoms. The above structures include all the possible configurations of the system $Nb_xAl_{1-x}N$. XRD spectra were calculated using the software PowderCell-2.4 [15].

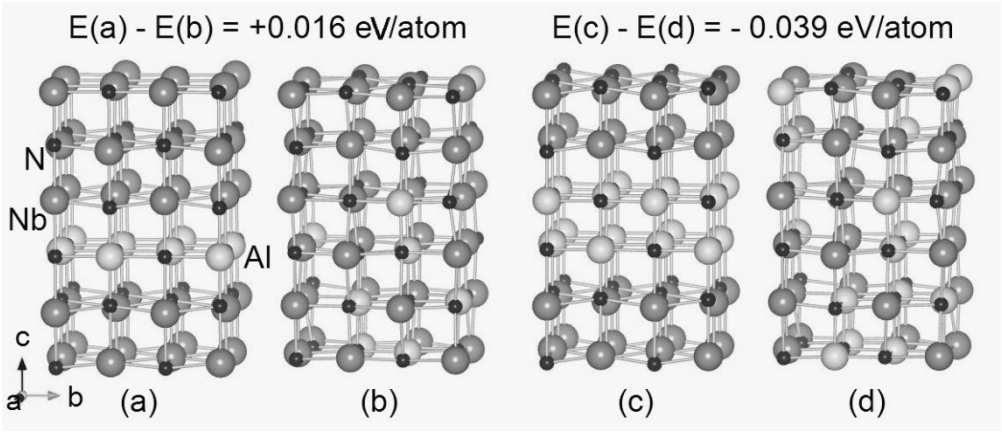

Fig. 4. Atomic configuration B1−NbN(001)/1 ML B1−AlN of heterostructure (a), of solid solution $Nb_{0.83}Al_{0.17}N$ (b), B1-NbN(001)/2 ML B1−AlN of heterostructure (c), of solid solution $Nb_{0.67}Al_{0.33}N$ (d).

Composition of structures (a) and (b) is the same; a structure composition (c) is equal to the composition respectively (d). The inscription above the figure represents the difference between the total heterostructure energies and the corresponding solid solution with a random arrangement of atoms in the metal lattice. Figure 4 shows the atomic configuration of heterostructures B1−NbN(001)/ 1 ML AlN and B1−NbN(001)/ 2 ML B1−AlN, ML-monolayer, as well as solid solutions B1−$Nb_xAl_{1-x}N$. Analysis of the total energies shows that solid solutions B1−$Nb_xAl_{1-x}N$ for x <0.67 should decay and nanocomposite structure with B1-AlN interface can be formed for these concentrations.

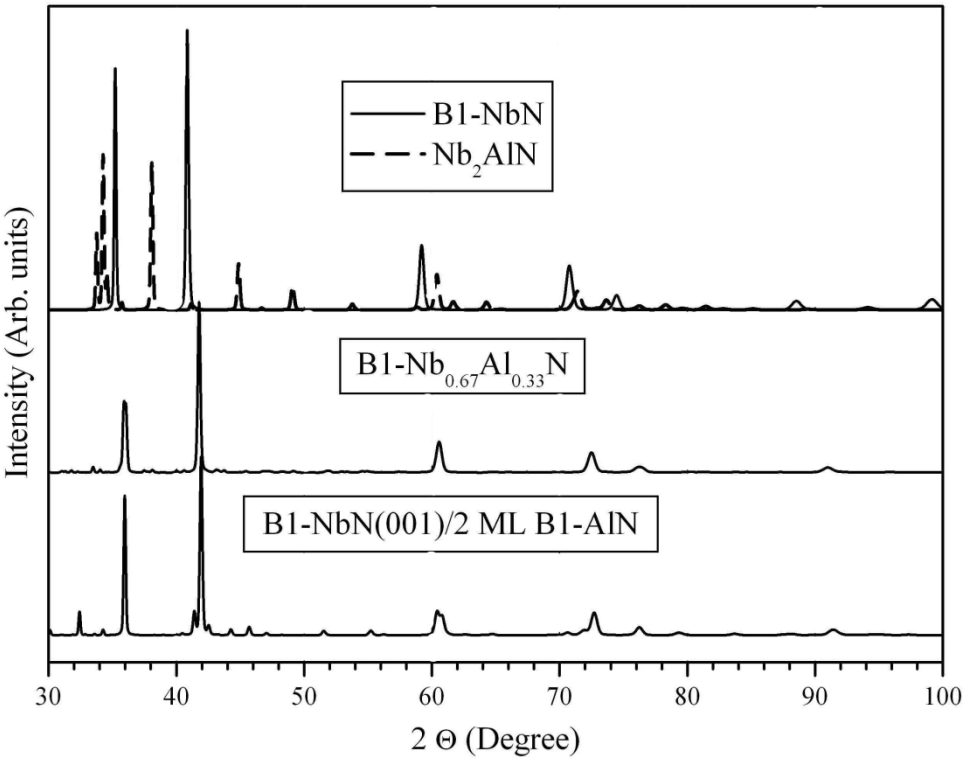

Fig. 5. The calculated X-ray diffraction patterns.

Using atomic configurations resulting from first-principles calculations, we calculated diffraction patterns for the B1−$NbN_ч$, B1−$Nb_xAl_{1-x}N$, x ~ 0.67 и Nb_2AlN. The calculated XRD spectra are shown in Figure 5. Comparison of the calculated and experimental spectra (Figure1) shows that reflexes about $2\Theta \sim 32^0$ associated with the heterostructure, and about $2\Theta \sim 38^0$, resulted by phase Nb_2AlN and does not occur at the experimental spectra. Therefore, we can assume that our films contain neither Nb_2AlN, nor any epitaxial layers B1-AlN, but rather consist of crystallites B1−NbN_{ch} and B1−$Nb_xAl_{1-x}N$, x ~ 0.67. As the matter of the fact the difference between the peak positions $\Delta 2\Theta = 2\Theta\cdot(B1-NbN_ч)-2\Theta\cdot(B1-Nb_xAl_{1-x}N)$ for each diffraction peak (200) and (400) on experimental and theoretical diffraction patterns is almost identical. We should also note that films of niobium nitride are prone to accumulate small amounts of oxygen [5]. Oxygen can replace part of the nitrogen in solid solution and in the amorphous matrix [16,17]. Therefore, structure $Nb_xAl_{1-x}N_yO_{1-y}$, x~0.67, 1-y << 1will be more realistic for the solid solutions, as for the amorphous matrix - a-AlNO, which was shown as a result of elemental analysis, obtained by SIMS, RBS and EDS in these films

CONCLUSION

Films Nb-Al-N were deposited on silicon substrates by magnetron sputtering targets of Nb and Al at different discharge powers at the target of aluminum. Experimental and theoretical studies show that the films obtained at selected deposition parameters have the nanocomposite structure that represents the nanocrystals B1−NbN_x and B1-$Nb_xAl_{1-x}N_yO_{1-y}$, embedded in a-AlNO matrix (nc−B1−NbN_x/nc−B1−Nb_xAl_{1-}

$_xN_eO_{1-y}$/a−AlNO). Nanocomposite coating with high microstrain action due to the difference in atomic radius of the crystal lattices metal components shows high hardness values (up to 32 GPa). Deposited nanocomposite films may be recommended with the given mechanical properties as wear resistant or protective coatings.

REFERENCES

[1] Barnett S A, Madan A, Kom I, Martin K 2003 *Mrs Bulletin*. 28, 169
[2] Gotoh Y, Nagao M, Ura T, Tsuji H, Ishikawa J 1999 *Nucl. Instr. Methods Phys. Res.* B **148**, 925
[3] Selinder T I, Miller D J, Gray K E 1995 *Vacuu*, **46**, 1401
[4] Makino Y, Saito K, Murakami Y, Asami K 2007 *Solid State phenomena* **127**, 195
[5] Barshilla H C, Deepthi B, Rajam K S. Mater J 2008 *Res.* **23**, 1258
[6] Franz R, Lechthaler M, Polzer C, Mitterer C 2010 *Surf. Coat. Technol.* **204**, 2447
[7] Holec D, Franz R, Mayrhofer P H, Mitterer C 2010 *J. Phys.* D **41**, 145403
[8] X-ray powder diffraction file [038-1155]
[9] Umanski Y S, Skakov Y A 1978 Physica metallov. Atomnoe stroenie metallov i splavov *Atomizdat M.* p 352
[10] Jadannadham K, Sharma A K, Wei Q, Kalyanraman R, Narayan 1998 *Vac. Sci. Technol* A **16**, 2804
[11] Ivashchenko V I, Veprek S, Scrynskyy P L, Lytvyn O, Butenko O O, Sinelnichenko O K, Gorb L, Hill F, Leszczynski J, Kozak A O 2014 *Superhard Materials* **36**, 1
[12] Ivashchenko V I, Veprek S, Turchi P E A, Shevchenko V I 2012 *Phys. Rev.* B **85,** 195403-1
[13] Giannozzi P, Baroni S, Bonini N, Calandra M, Car R, Cavazzoni C, Ceresoli D, Chiarotti G L, CococcioniI M. Dabo, Dal Corso A, de Gironcoli S, Fabris S, Fratesi G, Gebauer R, Gerstmann U, Gougoussis C, Kokalj A, Lazzeri M, Martin-Samos L, Marzari N, Mauri F, Mazzarello R, Paolini S, Pasquarello A, Paulatto L, Sbraccia C, Scandolo S, Sclauzero G, Seitsonen A P, Smogunov A, Umari P, Wentzcovitch R M 2009 *Phys.: Cond. Matter* **21,** 395502-19
[14] Perdew J P, Burke K, Ernzerhof M 1996 *Phys. Rev. Lett.* **77,** 3865
[15] Kraus W, Nolze G 2000 PowderCell for Windows, version 2.4
[16] Ivashchenko V, Veprek S, Pogrebnjak A,Postolnyi B 2014 *Sci. Tech. Adv. Mater*. **15,** 025007-11
[17] Pogrebnjak A D, Bagdasaryan A A, Yakushchenko I V, Beresnev V M 2014 *Rus. Chem. Rev.* **83**, 1027